J Mater Sci: Mater Electron (2017) 28:13236–13246
DOI 10.1007/s10854-017-7159-0

Surfactant-free hydrothermal synthesis of flower-like BiOBr hierarchical structure and its visible light-driven catalytic activity towards the degradation of sunset yellow

Jin-Chung Sin[1] · Chin-Aik Lim[1] · Sze-Mun Lam[2] · Abdul Rahman Mohamed[3]

Received: 7 March 2017 / Accepted: 15 May 2017 / Published online: 19 May 2017

Abstract Flower-like BiOBr hierarchical structures were successfully prepared by a facile and surfactant-free hydrothermal method. The as-synthesized products were characterized by X-ray diffraction (XRD), energy-dispersive X-ray spectroscopy (EDX), field-emission scanning electron microscopy (FESEM), transmission electron microscopy (TEM), X-ray photoelectron spectroscopy (XPS) and UV–Visible diffuse reflectance spectroscopy (UV–Vis DRS). The characterization results showed that the as-synthesized products were tetragonal phase pure BiOBr and demonstrated well-crystalline with good optical properties. It was also observed that the as-synthesized products were accumulated by large amount of interleaving nanosheets and formed an open porous structure through oriented aggregation. Under visible light irradiation, the as-synthesized products exhibited much higher photocatalytic activity compared to commercial TiO_2-P25 for sunset yellow degradation. Such enhancement was attributed to the unique hierarchical porous surface structure of flower-like BiOBr with good visible light absorption ability which can enhance the generation and separation of electron–hole pairs and led to high yield of hydroxyl radicals quantities as evidenced by the photoluminescence spectra. Moreover, the photocatalytic studies showed that various effects of parameters exerted their individual influence on the degradation of sunset yellow. Furthermore, the as-synthesized products were reused several times without appreciable loss of activity, showing great potential for practical applications in environmental remediation.

1 Introduction

Nowadays, environmental pollution caused by the continuous discharge of industrial effluents containing dyes, phenols, pesticides, solvents and other organic pollutants has become major problems for human society and seriously threaten the existence of terrestrial lives. Most of them were highly resistant to biodegradation and may undergo natural reductive anaerobic degradation to produce potentially carcinogenic intermediates [1]. Sunset yellow (SSY) is considered as one of the important organic dyes which widely used in food, cosmetic and pharmaceutical industries. In China, SSY was severely used as additives to food products to impart orange or red colour due to some toxicity cases [2]. In 2013, Ministry of Health Malaysia has also discovered a case of SSY contamination on poultry meat products which resemble chicken to deceive consumers [3]. Numerous studies have also shown that SSY exhibited toxicity, mutagenic, genotoxic and carcinogenic properties [3, 4]. The observed SSY effect came from chromosomal aberration in the liver and germinative cells, DNA fragmentation and increase of morphological abnormalities in spermatozoids of mice [4]. The photocatalysis with UV-irradiated TiO_2 has become an effective method to convert organic pollutants into nontoxic molecules to eliminate the

✉ Jin-Chung Sin
sinjc@utar.edu.my

[1] Department of Petrochemical Engineering, Faculty of Engineering and Green Technology, Universiti Tunku Abdul Rahman, Jalan Universiti, Bandar Barat, 31900 Kampar, Perak, Malaysia

[2] Department of Environmental Engineering, Faculty of Engineering and Green Technology, Universiti Tunku Abdul Rahman, Jalan Universiti, Bandar Barat, 31900 Kampar, Perak, Malaysia

[3] School of Chemical Engineering, Universiti Sains Malaysia, Engineering Campus, 14300 Nibong Tebal, Pulau Pinang, Malaysia

environmental pollution. However, given the wide band gap of TiO_2 (~3.2 eV), it is not that much effective for photocatalytic application under visible light which limited its practical applications [5, 6]. Thus, the exploitation of alternative photocatalysts that are responsive to UV and visible light is indispensable for the practical application of the photocatalytic system.

The ternary oxide semiconductor of bismuth oxyhalides has recently received enormous scientific attention due to their excellent optical properties and wide potential applications as catalysts, ferroelectric materials and pigments [7–9]. Among them, BiOBr is of great research interest for its excellent performance as UV and visible light-driven photocatalysts for the degradation of various organic pollutants in both air and aqueous media [9–11]. The hybridization between Bi 6s and O 2p states can narrow the band gap of BiOBr and extended the light absorption to visible light region. In addition, the unique layered tetragonal matlockite structure with $[Bi_2O_2]$ slabs interleaved by double slabs of bromine atoms endowed BiOBr with high carrier mobility and efficient photogenerated electron–hole pairs separation, which were beneficial to the photocatalytic activity [9]. Hitherto, BiOBr with different morphologies and structures have been fabricated including nanosheets, nanoplates, nanobelts, clover-shaped, hierarchical and complex BiOBr micro-architectures [10–13]. In particular, three-dimensional (3D) BiOBr hierarchical structures assembled from low-dimensional nanoscale building blocks have become a class of attractive materials due to their peculiar structure and unique properties. Previous studies have demonstrated that BiOBr hierarchical structures exhibited better photocatalytic activity as they were more structurally stable and can provide larger number of surface activation sites for the diffusion and mass transportation of organic molecules and reactive radicals in the photocatalytic degradation [14, 15]. Till now, most of the BiOBr with hierarchical structures were developed via the surfactants or templates assisted route, and assemblage of nanoscaled building blocks into the 3D structured morphologies without any surfactants still remains an intricate challenge.

On the basis of the above consideration, this work reports for the first time on the synthesis of BiOBr hierarchical structure with flower-like morphology via a simple hydrothermal route without any surfactant or templates. The structural, morphological and optical properties of the as-synthesized BiOBr products were characterized using the XRD, EDX, FESEM, TEM, XPS and UV–Vis DRS measurements. A possible mechanism for formation of the hierarchical structures was also discussed. The as-synthesized flower-like BiOBr hierarchical structures were used as photocatalysts for SSY degradation under visible light irradiation. To the best of our knowledge, this is the first work reporting photocatalytic degradation of this compound with flower-like BiOBr hierarchical structures. It is believed that this will be the pioneering work on the catalytic properties, photocatalytic activity and reusability of the flower-like BiOBr hierarchical structures on SSY degradation. Moreover, the effects of BiOBr amount, initial substrate concentration as well as solution pH on the photocatalytic activities of flower-like BiOBr hierarchical structures were investigated. Enhancement of photocatalytic activity was also observed when as-synthesized BiOBr products were used as photocatalysts compared to commercial TiO_2-P25.

2 Experimental

2.1 Preparation of flower-like BiOBr hierarchical structures

All the reagents were of analytical grade without further purification. The detailed synthesis procedure was as follows: 4 mmol $Bi(NO_3)_3{\cdot}5H_2O$ was dissolved into 80 mL acetic acid and labeled as solution (A) Meanwhile, 4 mmol KBr was dissolved into 40 mL deionized water and labeled as solution (B) Then the solution A was added drop-wise into the solution B under stirring. The resulting mixed solution was transferred to a Teflon-lined autoclave and maintained at 120 °C for 12 h. The as-formed products were filtrated, washed with deionized water and ethanol, dried at 80 °C for 8 h and finally calcined at 400 °C for 3 h.

2.2 Characterization

The as-synthesized products were characterized by X-ray diffraction (XRD) analysis on a Philips PW1820 diffractometer equipped with Cu Kα radiation over a range of 10° to 70°. The field emission scanning electron microscopy (FESEM) analysis was performed using a JEOL JSM-6701F together with an energy dispersion X-ray spectrum (EDX) analysis. Transmission electron microscopy (TEM) image was taken on a Philips CM 12 instrument operating at 120 keV. The X-ray photoelectron spectroscopy (XPS) spectra were obtained on a PHI Quantera II. Diffuse reflectance spectroscopy (DRS) of catalysts was tested in a Perkin Elmer Lambda 35 UV–Vis spectrometer. The spectra were recorded timely in the range of 350–700 nm using $BaSO_4$ as the reference standard.

2.3 Measurement of photocatalytic activity

The photocatalytic activity of the as-synthesized BiOBr products was evaluated by the degradation of SSY in water. Experiment was as follows: an appropriate amount of catalyst was dispersed in 200 mL of solution containing known

concentration of SSY that adjusted to a desired initial pH value. During all experiments, air was bubbled into the solution at a constant flow rate of 2 mL/min. The suspensions were continuously stirred with the aid of a magnetic stirrer. The heterogeneous mixture was equilibrated for 30 min in the dark. The SSY concentration after equilibration was monitored using a UV–Vis spectrophotometer at 480 nm and taken as initial concentration (C_o). Then, the solution was irradiated under a 55 W compact fluorescent lamp. The average light intensity striking the surface of the reaction solution was about 14,500 lx, as measured by a digital luxmeter. This lamp was fixed about 10 cm above the reaction solution. The photocatalytic reaction temperature was kept at room temperature using cooling fans to prevent any thermal catalytic effect. After the elapse of a period of time, 4 mL of the solution was withdrawn from the system and the concentration of SSY (C) was determined. Meanwhile, the comparison studies with commercial TiO_2-P25 were also carried out. The durability test of the as-synthesized BiOBr products was also conducted using the same procedure as above and the products underwent four consecutive cycles, each lasting for 180 min. After each cycle, the catalysts were centrifuged and washed thoroughly with water, and then added to fresh SSY solution. In order to determine the reproducibility of all the results, at least duplicated runs were conducted for each condition for averaging the results, and the experimental error was found to be within ±4%.

2.4 Analysis of hydroxyl radicals (·OH)

Terephthalic acid photoluminescence probing technique (TA-PL) was carried out to detect the ·OH. Terephthalic acid readily reacted with ·OH to produce highly fluorescent product, 2-hydroxyterephthalic acid. The method relied on the PL signal at 425 nm of 2-hydroxyterephthalic acid. The PL intensity of 2-hydroxyterephthalic acid was proportional to the amount of ·OH formed. In the TA-PL experiment, a basic terephthalic acid solution was added to the reactor instead of SSY and the concentration of terephthalic acid was set at 5×10^{-4} M in 2×10^{-3} M NaOH solution. The PL spectra of generated 2-hydroxyterephthalic acid were measured by a Perkin-Elmer Lambda S55 spectrofluorometer. At the given irradiation time, the reaction solution was used to measure the PL intensity at 425 nm by excitation with a wavelength of 315 nm.

3 Results and discussion

3.1 Characterization of the as-synthesized products

Figure 1a shows the XRD pattern of as-synthesized products. All the diffraction peaks were labeled and can be assigned to the tetragonal phase of BiOBr (JCPDS no. 09-0393) with lattice parameters of $a=3.92$ Å, $c=8.10$ Å. No other diffraction peaks were detected in the pattern, indicating the high purity and single phase of the products. The intense and sharp diffraction peaks also showed that the obtained BiOBr were well crystalline. The average crystallite size (D) of the products was calculated to be 45 nm according to the Scherrer equation $D=0.9\lambda/(\beta\cos\theta)$, where λ is the wavelength of the incident X-ray radiation, β is the full width at half maximum (FWHM) and θ is the Bragg angle [16]. Further evidence of the formation of BiOBr came from the EDX analysis, which unambiguously

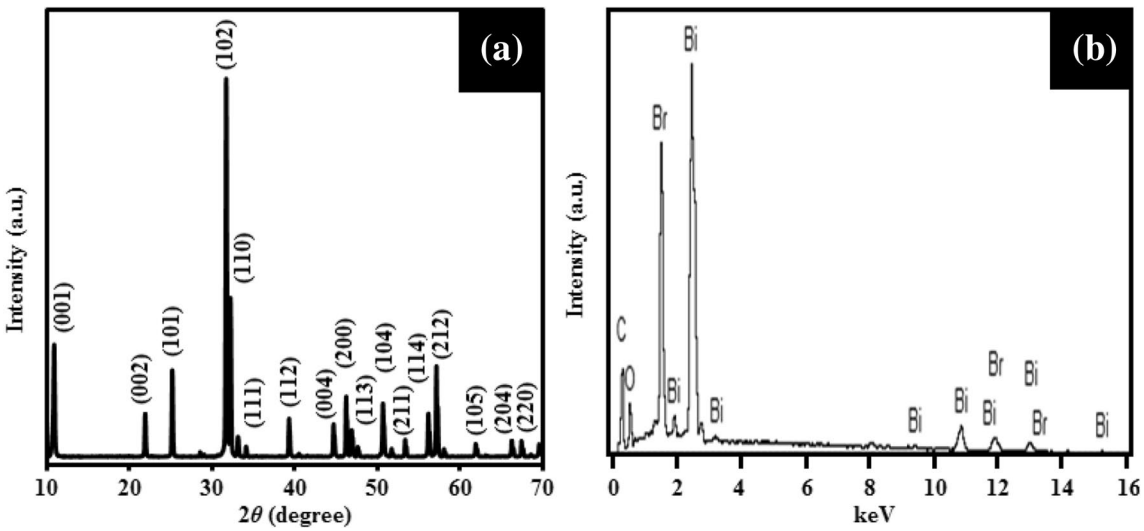

Fig. 1 **a** XRD pattern and **b** EDX spectrum of as-synthesized flower-like BiOBr hierarchical structures

demonstrated the products contained Bi, O and Br elements (Fig. 1b). The C element in the EDX was originated from the supporting carbon tape.

Figure 2 shows the FESEM and TEM images of the as-synthesized products. The panoramic morphology of the products is presented in Fig. 2a, indicating the synthesized products were flower shaped and had sizes in the range of several hundred nanometers to micrometers. The magnified images in Fig. 2b, c showed that the microflowers had hierarchical structure assembled by lots of interleaving nanosheets of average thickness of ~80 nm and formed an open porous structure through oriented aggregation. Figure 2d demonstrated the TEM image of the product consisted of nanosheets which were arranged in such an order way to form flower-shaped morphologies. The TEM observation of the as-synthesized BiOBr products further confirmed the FESEM investigations.

In the present system, $Bi(NO_3)_3{\cdot}5H_2O$ firstly reacted with acetic acid to form $Bi(CH_3COO)_3$ in solution (A) Meanwhile, the addition of KBr into water can dissociate Br^- ions in solution (B) When both A and B solutions were mixed together, the $Bi(CH_3COO)_3$ reacted with water to form $BiO(CH_3COO)$. The Br^- ions in solution can then react with $BiO(CH_3COO)$ to form BiOBr nuclei via anion exchange process and followed by a crystal growth process. The reaction process can be expressed as follows:

$$Bi^{3+} + 3CH_3COOH \rightarrow Bi\left(CH_3COO\right)_3 + 3H^+ \quad (1)$$

$$KBr + H_2O \rightarrow KOH + H^+ + Br^- \quad (2)$$

$$Bi\left(CH_3COO\right)_3 + H_2O \rightarrow BiO\left(CH_3COO\right) + 2CH_3COOH \quad (3)$$

$$BiO\left(CH_3COO\right) + Br^- \rightarrow BiOBr + CH_3COO^- \quad (4)$$

With the reaction proceeding, these nuclei could serve as the sites for the growth of BiOBr nanosheets by grew anisotropically along the 2D directions [17]. Thermodynamically, the surface energy of an individual nanosheet was quite high with two main exposed planes and thus they tended to aggregate into larger grains via self-organization of adjacent nanosheets leading a 3D assembly process to decrease the surface energy by reducing exposed areas. Therefore, the flower-like BiOBr hierarchical structure was constructed from the nanosheets by oriented aggregation processes. Scheme 1 shows the

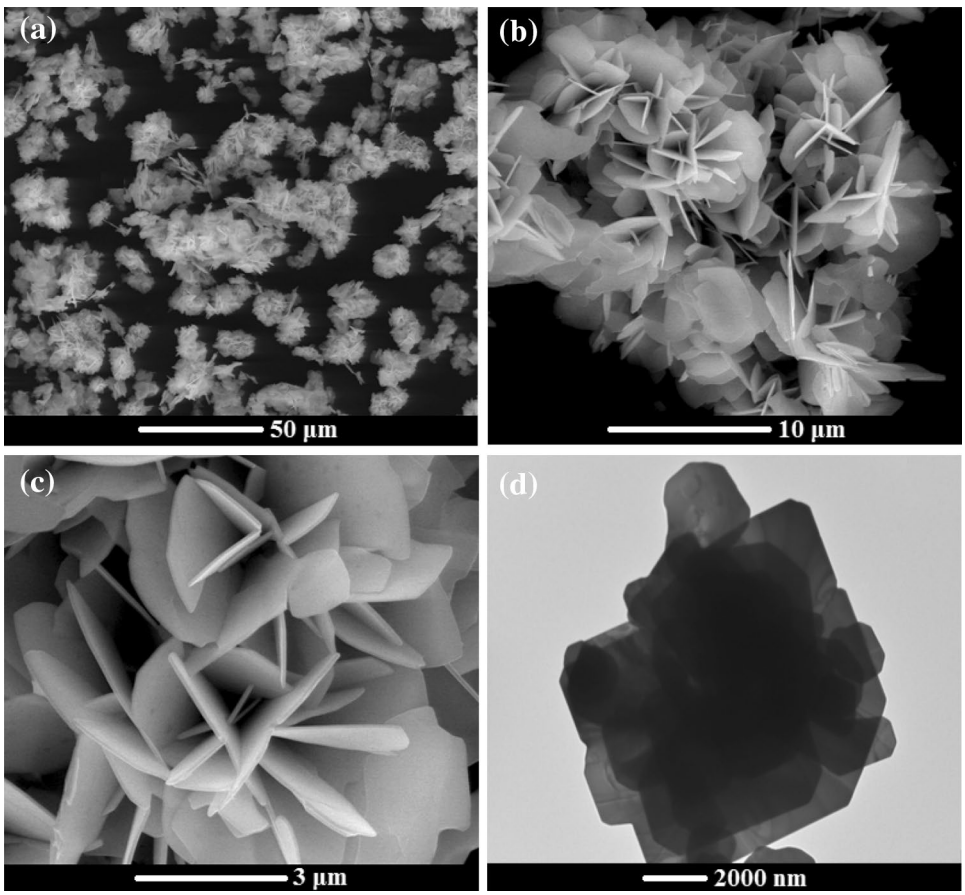

Fig. 2 **a–c** FESEM images and **d** TEM image of as-synthesized flower-like BiOBr hierarchical structures

Scheme 1 Schematic illustration of the formation process of flower-like BiOBr hierarchical structures

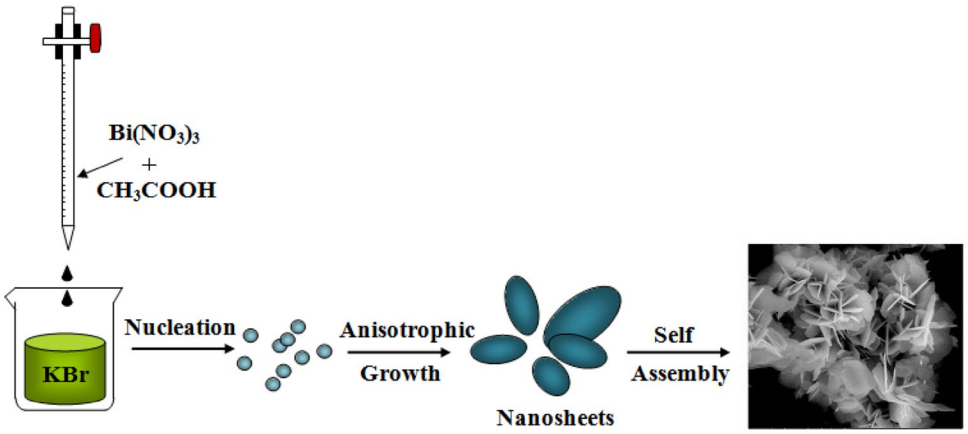

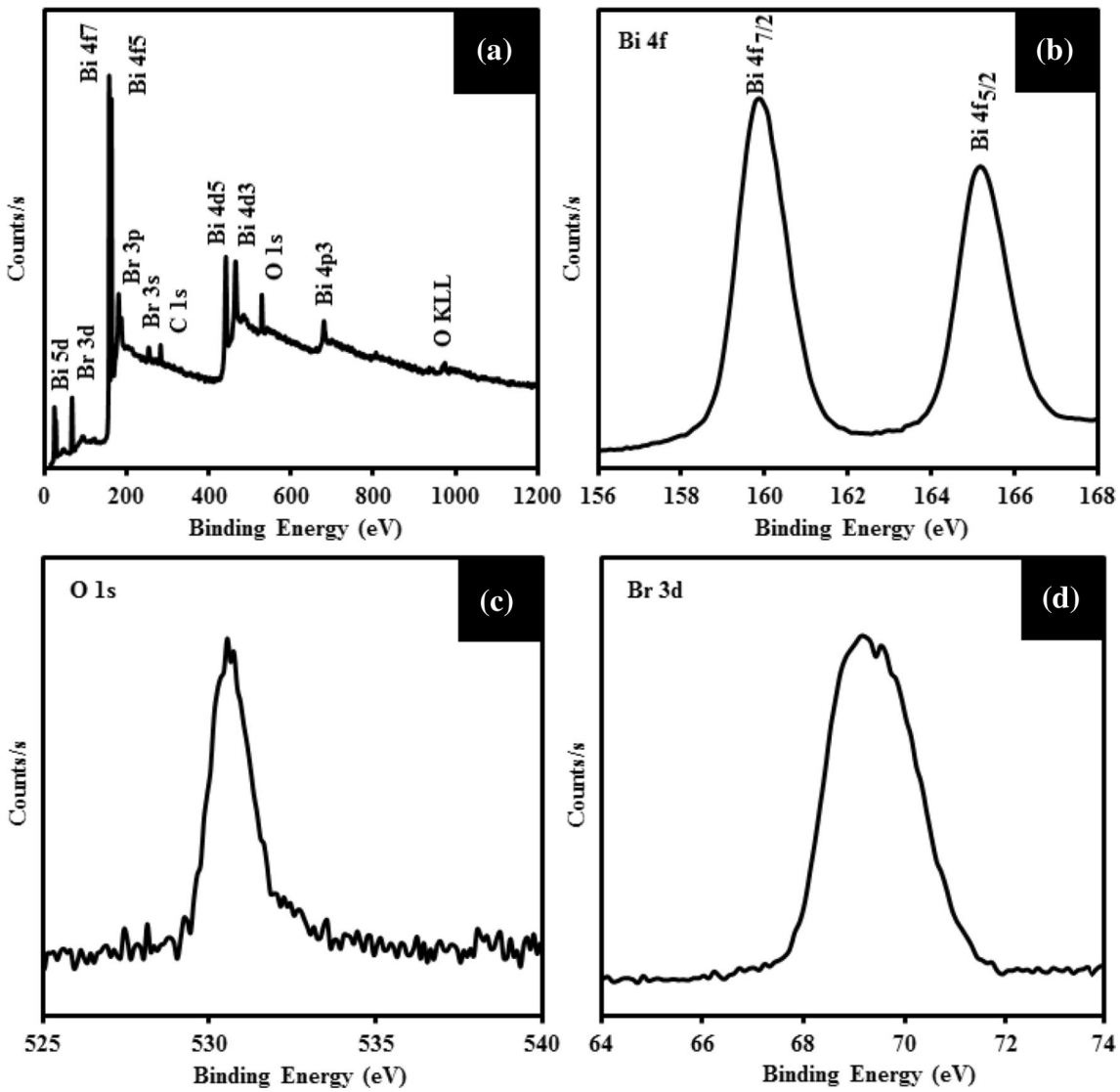

Fig. 3 XPS spectra of as-synthesized flower-like BiOBr hierarchical structures: **a** survey, **b** Bi 4f, **c** O 1s and **d** Br 3d

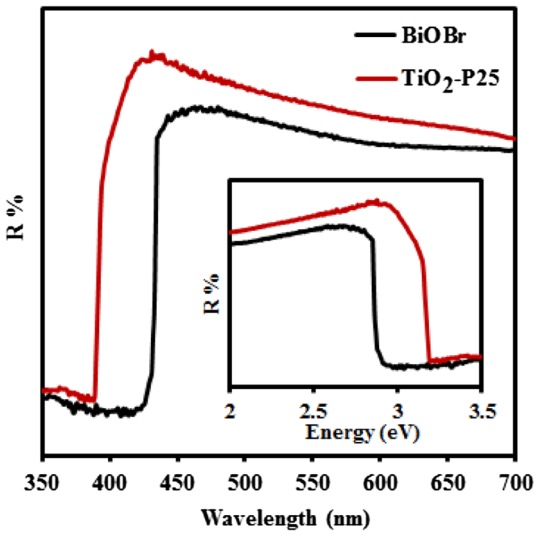

Fig. 4 UV–Vis DRS spectra of as-synthesized flower-like BiOBr hierarchical structures and commercial TiO_2-P25. The *inset* shows the plot of R% versus photon energy

schematic illustration of the formation process of flower-like hierarchical structure. In our work, the 3D BiOBr structures with nanosheets were fabricated without any surfactant and template, and it is also a facile way for large-scale synthesis of 3D BiOBr structures.

Figure 3a shows the XPS spectrum of as-synthesized products. The products were composed of Bi, O and Br elements, which further confirmed the synthesized products were pure BiOBr. A trace amount of carbon in the results was mainly attributed to the adventitious hydrocarbon from XPS itself [18]. Figure 3b–d show the high resolution XPS spectra of the elements of Bi, O and Br. The Bi 4f region (Fig. 3b) was displayed with the symmetrical peaks at 159.9 and 165.1 eV were corresponded to the Bi $4f_{7/2}$ and Bi $4f_{5/2}$, respectively, which indicated the chemical states of bismuth element were trivalent [19, 20]. In Fig. 3c, the peak located at 530.3 eV was attributed to O^{2-} in BiOBr [20]. The Br 3d peak was associated with binding energy of 69.2 eV (Fig. 3d), which was the characteristic of Br^- in BiOBr [21].

Figure 4 shows the UV–Vis DRS spectrum of the as-synthesized products. The commercial TiO_2-P25 which was the common used photocatalyst was also shown as comparison. It was noticeable that the light absorption of the synthesized flower-like BiOBr hierarchical structures in the visible light region was higher than that of TiO_2-P25, suggesting their potential photocatalytic activity under visible light. The band gap energy of as-synthesized BiOBr products was calculated using the equation E_g (eV) = 1240/λ (nm), where λ is the wavelength (nm) of absorption onset and E_g is the band gap energy of synthesized products [22]. The E_g was determined to be 2.88 eV (inset of Fig. 4), which was lower than that of TiO_2 (3.24 eV). Above results also revealed that the synthesized flower-like BiOBr hierarchical structures can absorb in UV as well as in visible light regions of the solar light. Therefore, the absorption property inferred that the as-synthesized BiOBr products have suitable band gap to be activated by visible light for photocatalytic reaction.

3.2 Photocatalytic activity

The photocatalytic activity of the as-synthesized products was evaluated by the SSY degradation under visible light irradiation. Figure 5a shows the degradation results in the presence of different amounts of flower-like BiOBr hierarchical structures. Blank experiment of SSY degradation in the absence of catalysts under the similar conditions was also carried out. The results revealed that the self-photolysis of SSY upon light irradiation can be neglected as the degradation efficiency was 3.0% after 180 min irradiation. However, the photocatalytic degradation of SSY occurred well in the presence of as-synthesized BiOBr products and light irradiation, indicating that the SSY degradation performed via the photo-activation of BiOBr. With the increase in BiOBr amount, the degradation efficiency of SSY firstly increased from 13.0% at 0.25 g/L to 53.5% at 1.00 g/L and then decreased to 43.9% at 2.00 g/L. This can be due to the fact that an increase in photocatalyst amount can result in more effective absorption of photons and adsorption of SSY moelcules, which enhanced the photocatalytic degradation. However, when the photocatalyst was overdosed, the intensity of light was attenuated owing to the decrease of light penetration and increase of light scattering, which counteracted the enhancement effect coming from the increase of photocatalyst amount and therefore decreased the photocatalytic efficiency [23].

Figure 5b shows the effect of initial substrate concentration on the photocatalytic degradation of SSY on 1.00 g/L flower-like BiOBr hierarchical structures. It was found that the increase of initial SSY concentration from 10 to 60 mg/L decreased the degradation efficiency from 53.5 to 8.1% after 180 min irradiation. The efficiency of degradation was related to the active species formation on catalyst surface and probability of active species reacting with SSY molecules. For all initial SSY concentrations, the photocatalyst amount and irradiation time were constant. Since the generation of active species remained the same, the probability of SSY molecules to react with the active species decreased. At high SSY concentrations, the large amount of adsorbed SSY can also compete with O_2 and OH^- onto the BiOBr surface, which suppressed the generation of active species for photocatalytic degradation. The increase in SSY concentration also decreased the path length of photon entering into the SSY solution and consequently fewer

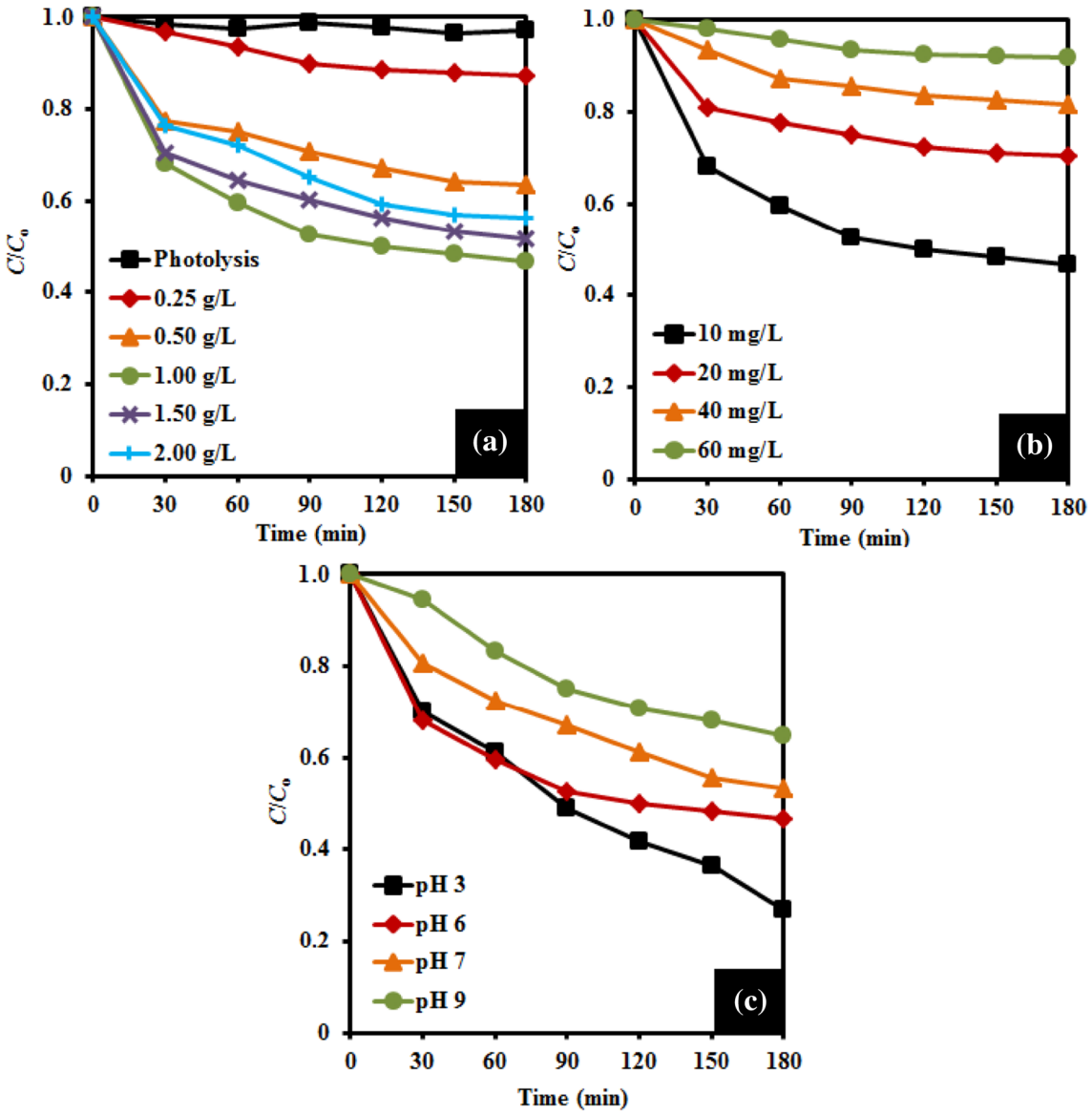

Fig. 5 **a** Effect of BiOBr amount on the photocatalytic degradation of SSY ([SSY] = 10 mg/L; pH 6). **b** Effect of initial substrate concentration on the photocatalytic degradation of SSY (BiOBr amount = 1.00 g/L; pH 6). **c** Effect of solution pH on the photocatalytic degradation of SSY (BiOBr amount = 1.00 g/L; [SSY] = 10 mg/L)

photons managed to activate the BiOBr surface essentially decreased the degradation efficiency [24, 25].

The effect of solution pH on the photocatalytic degradation of SSY was also studied by varying the initial pH of aqueous SSY solution from 3 to 9 with aqueous H_2SO_4 or NaOH solutions while keeping all other experimental conditions constant (BiOBr amount of 1.00 g/L and SSY concentration of 10 mg/L). As shown in Fig. 5c, the degradation efficiency gradually increased with increasing irradiation time at all investigated pH value. After 180 min, the degradation efficiency of SSY reached maximum value at pH 3, while the degradation efficiencies dropped from 73.3 to 53.5%, 46.7 and 35.1% with the further increase in pH to 6 (natural pH), 7 and 9, respectively. The interpretation of pH effects on the efficiency of SSY photodegradation process was related to the electrical charge properties of both photocatalyst and substrate. It was noted that at pH 3, the surface of flower-like BiOBr hierarchical structures was positively charge because the zero potential point of BiOBr was 3.4 [26]. Since SSY has an anionic configuration, the electrostatic attraction between positively charged BiOBr with anionic SSY led to maximum degradation efficiency. On the other hand, at higher pH, the BiOBr surface became negatively charged and developed repulsive forces between the deprotonated catalyst and the anionic SSY. Thus, due to

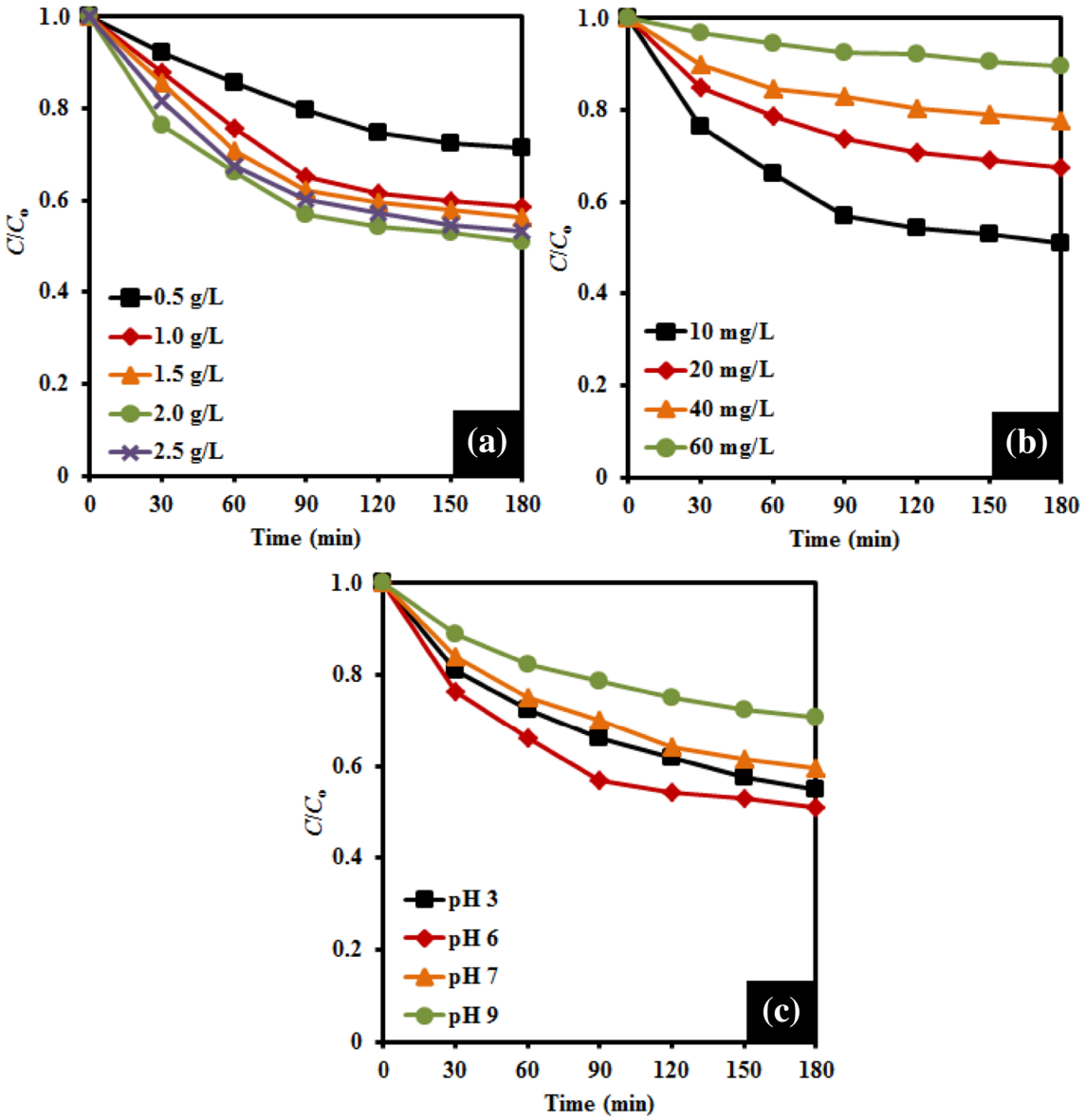

Fig. 6 **a** Effect of TiO_2-P25 amount on the photocatalytic degradation of SSY ([SSY] = 10 mg/L; pH 6). **b** Effect of initial substrate concentration on the photocatalytic degradation of SSY (TiO_2-P25 amount = 2.0 g/L; pH 6). **c** Effect of solution pH on the photocatalytic degradation of SSY (TiO_2-P25 amount = 2.0 g/L; [SSY] = 10 mg/L)

Coulombic repulsion, the SSY was scarcely adsorbed and resulted in lower photocatalytic activity [23, 27].

For comparison, the effects of photocatalyst amount, initial substrate concentration and solution pH on the degradation of SSY were also investigated using commercial TiO_2-P25 as photocatalyst. The optimum photocatalyst amount was observed to be 2.0 g/L and the efficiency of degradation of SSY also decreased with the increase of initial substrate concentration. The degradation of SSY reached maximum efficiency at pH 6, which was the natural value of the aqueous SSY (Fig. 6). Figure 7 shows the comparative evaluation of flower-like BiOBr hierarchical structures and commercial TiO_2-P25 for the degradation of SSY. Under the optimized conditions, it can be found that the flower-like BiOBr hierarchical structures exhibited much higher photocatalytic performance than the commercial TiO_2-P25 (49.2% degradation efficiency). Such photocatalytic enhancement over flower-like BiOBr hierarchical structures can be explained by the efficient separation of electron–hole ($e_{cb}^{-}-h_{vb}^{+}$) pairs and generation of large number of $e_{cb}^{-}-h_{vb}^{+}$ pairs under light irradiation. In our study, BiOBr has greater absorption in both UV and visible light regions which can increase the quantity of photogenerated $e_{cb}^{-}-h_{vb}^{+}$ pairs available to participate in the

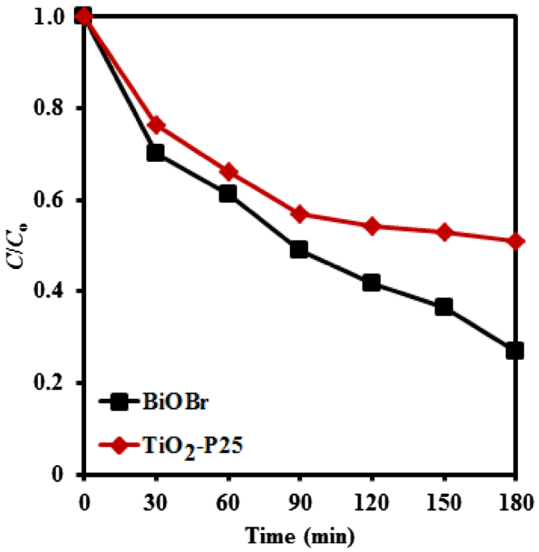

Fig. 7 Photocatalytic performances of as-synthesized flower-like BiOBr hierarchical structures and commercial TiO_2-P25 for SSY degradation under optimized conditions

photocatalytic degradation of SSY. In addition, the unique hierarchical porous surface structure of flower-like BiOBr with good crystallinity also can increase the number of surface activation sites and allowed the efficient transport of photogenerated e_{cb}^-–h_{vb}^+ pairs to the substrate molecules. These factors are beneficial to form more active species such as ·OH to enhance the photocatalytic degradation of SSY as inferred from the following PL test in this study and other reports [28, 29].

3.3 Photocatalytic mechanism

Combining our experiment results with the related literatures [25, 30, 31], a plausible schematic illustration for SSY degradation over the flower-like BiOBr hierarchical structures could be proposed in Scheme 2. Under the irradiation, the e_{cb}^- are excited from the valence band to the conduction band of BiOBr leaving behind h_{vb}^+. The photogenerated h_{vb}^+ can trap on the catalyst surface undergoing charge transfer with absorbed water molecules or with surface-bound hydroxide species to generate active ·OH. At the same time, the photogenerated e_{cb}^- can be transferred to O_2 species to form H_2O_2. Then, cleavage of H_2O_2 by the e_{cb}^- further produced the ·OH and OH^- ions. The ·OH have been formed by many semiconductors like TiO_2 and ZnO via generation of e_{cb}^-–h_{vb}^+ pairs under irradiation [1, 31], which acted as strong oxidizing agents to degrade the organic pollutants. The photocatalytic mechanism of flower-like BiOBr hierarchical structures can be given as:

$$\mathrm{BiOBr} + h\nu \rightarrow \mathrm{BiOBr}\left(e_{cb}^- + h_{vb}^+\right) \quad (5)$$

$$h_{vb}^+ + \mathrm{H_2O} \rightarrow \cdot\mathrm{OH} + \mathrm{H^+} \quad (6)$$

$$h_{vb}^+ + \mathrm{OH^-} \rightarrow \cdot\mathrm{OH} \quad (7)$$

$$\mathrm{O_2} + 2\mathrm{H^+} + 2e_{cb}^- \rightarrow \mathrm{H_2O_2} \quad (8)$$

$$\mathrm{H_2O_2} + e_{cb}^- \rightarrow \cdot\mathrm{OH} + \mathrm{OH^-} \quad (9)$$

The above proposed photocatalytic mechanism was further confirmed by the detection of ·OH using TA-PL technique. Figure 8a shows the PL spectral changes observed after each photocatalyst was irradiated for 180 min irradiation in the aqueous basic solution of TA. An obvious PL signal was observed at 425 nm over both photocatalysts, demonstrating that ·OH were formed and participated in photocatalytic degradation process. It was also clear that the flower-like BiOBr hierarchical structures exhibited higher PL intensity than the commercial TiO_2-P25. This implied the flower-like BiOBr hierarchical structures can produce higher amount of ·OH and favourable for improving the photocatalytic activity compared to TiO_2-P25. The same results were also verified in Sect. 3.2. Moreover, Fig. 8b shows the change of PL spectra with irradiation time for the case of flower-like BiOBr hierarchical

Scheme 2 Schematic diagram of the photocatalytic mechanism of flower-like BiOBr hierarchical structures

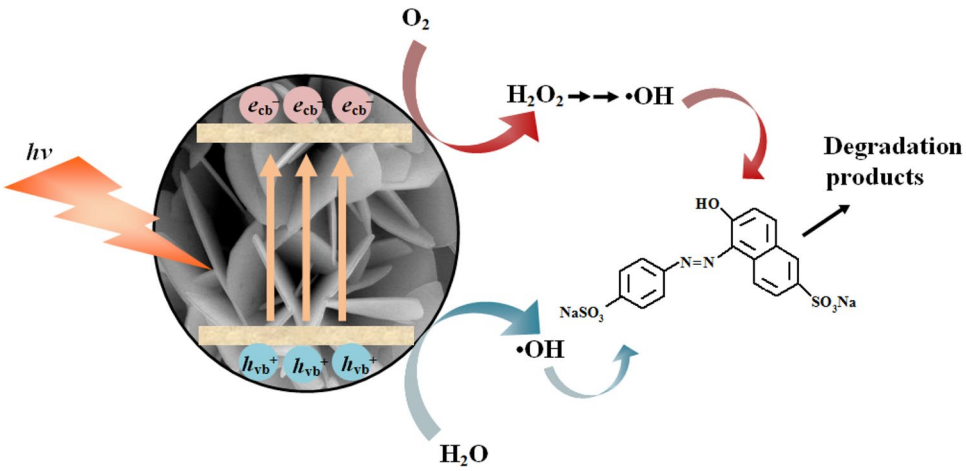

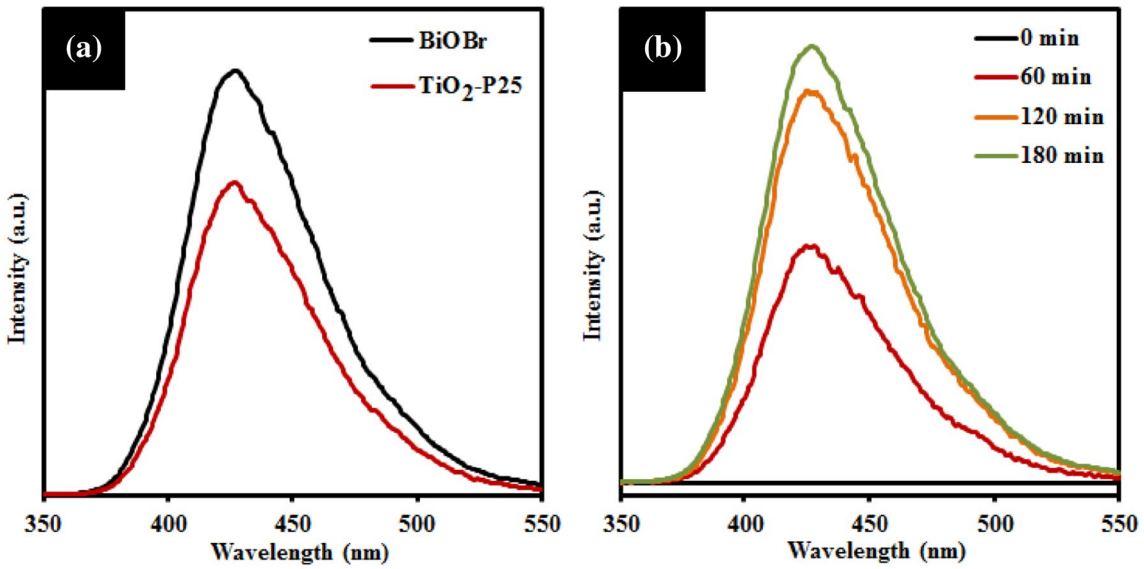

Fig. 8 **a** PL spectra of aqueous basic solution of TA with an excitation at 315 nm for as-synthesized flower-like BiOBr hierarchical structures and commercial TiO_2-P25. **b** PL spectra changing with irradiation time for the case of the flower-like BiOBr hierarchical structures

structures. A gradual increase in PL intensity was observed with increasing irradiation time, suggesting that the fluorescence was caused by chemical reactions of TA with ·OH formed during photoilluminated reactions. Thus, these results further confirmed the evidence of ·OH formation and indeed participated in the degradation process. Ultimately, the as-synthesized flower-like BiOBr still maintained high photocatalytic activity after four cycles (Fig. 9). This result suggested that the flower-like BiOBr hierarchical structures can be utilized as efficient photocatalysts for the degradation of organic dyes.

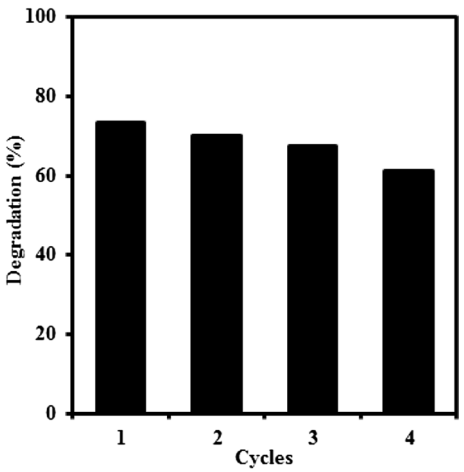

Fig. 9 Recycling efficiency of flower-like BiOBr hierarchical structures ([SSY] = 10 mg/L; BiOBr amount = 1.00 g/L; pH 3)

4 Conclusions

Flower-like BiOBr hierarchical structures were successfully fabricated via a simple and surfactant-free hydrothermal method. Detailed morphological observation revealed that the flower-like BiOBr was composed by lots of interleaving nanosheets of average thickness ~80 nm and formed an open porous structure through oriented aggregation. A possible mechanism of formation of the hierarchical structures was discussed. Detailed structural and optical characterization showed that the as-synthesized BiOBr had a highly crystalline tetragonal structure with good optical properties. The investigation of photocatalytic activities showed that the flower-like BiOBr hierarchical structures were differently affected by BiOBr amount, initial substrate concentration and solution pH. Compared to commercial TiO_2-P25 and none of catalyst, the as-synthesized BiOBr products showed much higher degradation efficiency of SSY under visible light irradiation. Such photocatalytic enhancement was attributed to the unique hierarchical porous surface structure of flower-like BiOBr with good visible light absorption ability which can enhance the generation and separation of $e_{cb}^{-}-h_{vb}^{+}$ pairs and led to high yield of OH quantities as evidenced by the photoluminescence spectra. Moreover, the as-synthesized flower-like BiOBr can be reused for several times without substantial loss of activity, which was favourable for potential practical applications.

Acknowledgements This research was supported by a UTAR Research Fund (UTARRF/2016-C2/S03) from Universiti Tunku

Abdul Rahman as well as Fundamental Research Grant Schemes (FRGS/1/2015/TK02/UTAR/02/2 and FRGS/1/2016/TK02/UTAR/02/1) through Ministry of Higher Education of Malaysia.

References

1. J.C. Sin, S.M. Lam, A.R. Mohamed, K.T. Lee, Int. J. Photoenergy **2012**, 185159 (2012)
2. Y. Xing, M. Meng, H.Y. Xue, T.C. Zhang, Y.M. Yin, R.M. Xi, Talanta **99**, 125 (2012)
3. K. Rovina, P.P. Prabakaran, S. Siddiquee, S.M. Shaarani, Trends Anal. Chem. **85**, 47 (2016)
4. H.M. Sayed, D. Fouad, F.S. Ataya, N.H.A. Hassan, M.A. Fahmy, Mutat. Res. **744**, 145 (2012)
5. Y.F. Wang, L. Yan, X.M. He, J. Li, D.J. Wang, J. Mater. Sci. **27**, 5190 (2016)
6. Y. Yao, L.X. Guan, Y. Ma, M.M. Yao, J. Mater. Sci. **28**, 3013 (2017)
7. D.S. Bhachu, S.J.A. Moniz, S. Sathasivam, D.O. Scanlon, A. Walsh, S.M. Bawaked, M. Mokhtar, A.Y. Obaid, I.P. Parkin, J.W. Tang, C.J. Carmalt, Chem. Sci. **7**, 4832 (2016)
8. Y.J. Si, J.B. Zhong, J.Z. Li, M.J. Li, L. Yang, J. Ding, Mater. Lett. **163**, 175 (2016)
9. V.J. Babu, M. Sireesha, R.S.R. Bhavatharini, S. Ramakrishna, Mater. Lett. **169**, 50 (2016)
10. Y.C. Feng, L. Li, J.W. Li, J.F. Wang, L. Liu, J. Hazard. Mater. **192**, 538 (2011)
11. Y. Liu, Y.Q. Yin, X.Q. Jia, X.Y. Cui, C.R. Tian, Y.H. Sang, H. Liu, Environ. Sci. Pollut. Res. **23**, 17525 (2016)
12. H.P. Li, J.Y. Liu, T.X. Hu, N. Du, S. Song, W.G. Hou, Mater. Res. Bull. **77**, 171 (2016)
13. X.L. Wang, J. Yang, Y.Y. Chen, Y.M. Zhang, Y. Tang, Mater. Lett. **116**, 171 (2014)
14. J.Y. Xiong, Q.S. Dong, T. Wang, Z.B. Jiao, G.X. Lu, Y.P. Bi, RSC Adv. **4**, 583 (2014)
15. Z.H. Ai, W.K. Ho, S.C. Lee, L.Z. Zhang, Environ. Sci. Technol. **43**, 4143 (2009)
16. J.C. Sin, S.M. Lam, K.T. Lee, A.R. Mohamed, J. Mol. Catal. A **409**, 1 (2015)
17. M. Shang, W.Z. Wang, L. Zhang, J. Hazard. Mater. **167**, 803 (2009)
18. S.M. Lam, J.C. Sin, A.Z. Abdullah, A.R. Mohamed, J. Colloid Interface Sci. **450**, 34 (2015)
19. D. Wu, S.T. Yue, W. Wang, T.C. An, G.Y. Li, H.Y. Yip, H.J. Zhao, P.K. Wong, Appl. Catal. B **192**, 35 (2016)
20. J.X. Xia, S. Yin, H.M. Li, H. Xu, L. Xu, Y.G. Xu, Dalton Trans. **40**, 5249 (2011)
21. Y. Zhao, X. Tan, T. Yu, S.C. Wang, Mater. Lett. **164**, 243 (2016)
22. J.C. Sin, S.M. Lam, K.T. Lee, A.R. Mohamed, Mater. Sci. Semicond. Process **16**, 1542 (2013)
23. J. Kaur, S. Singhal, Phys. B **450**, 49 (2014)
24. N. Rana, S. Chand, A.K. Gathania, J. Mater. Sci. **27**, 2504 (2016)
25. S.M. Lam, J.C. Sin, A.Z. Abdullah, A.R. Mohamed, Desalin. Water Treat. **41**, 131 (2012)
26. X.F. Chang, M.A. Gondal, A.A. Al-Saadi, M.A. Ali, H.F. Shen, Q. Zhou, J. Zhang, M.P. Du, Y.S. Liu, G.B. Ji, J. Colloid Interface Sci. **377**, 291 (2012)
27. U.I. Gaya, A.H. Abdullah, M.Z. Hussein, Z. Zainal, Desalination **263**, 176 (2010)
28. J. Xu, L. Li, C.S. Guo, Y. Zhang, S.F. Wang, Chem. Eng. J. **221**, 230 (2013)
29. J. Xu, W. Meng, Y. Zhang, L. Li, C.S. Guo, Appl. Catal. B **107**, 355 (2011)
30. Y. Wang, Z.Q. Shi, C.M. Fan, X.W. Wang, X.G. Hao, Y.Q. Chi, J. Solid State Chem. **199**, 224 (2013)
31. S.M. Lam, J.C. Sin, A.Z. Abdullah, A.R. Mohamed, Sep. Purif. Technol. **132**, 378 (2014)